JOURNAL OF Materials CHEMISTRY

Structure–property relationships in pyrochlores: low-temperature structures of $Tl_2Ru_2O_{7-\delta}$ ($\delta = 0.00$ and 0.05)†

T. Takeda,[a] R. Kanno,*[a] Y. Kawamoto,[a] M. Takano,[b] F. Izumi,[c] A. W. Sleight[d] and A. W. Hewat[e]

[a]*Department of Chemistry, Faculty of Science, Kobe University, Nada, Kobe, Hyogo 657, Japan*
[b]*Institute for Chemical Research, Kyoto University, Uji, Kyoto 611, Japan*
[c]*National Institute for Research in Inorganic Materials, 1–1, Namiki, Tsukuba, Ibaraki 305, Japan*
[d]*Department of Chemistry, Oregon State University, Corvallis, OR 97330, USA*
[e]*Institut Max von Laue-Paul Langevin, BP 156, F-38042 Grenoble Cedex 9, France*

Received 8th June 1998, Accepted 21st July 1998

Structural, electrical and magnetic properties are investigated for ruthenium pyrochlores. The structure of the thallium ruthenium pyrochlore, $Tl_2Ru_2O_{7-\delta}$, has been determined for $\delta = 0.00$ and 0.05 by neutron diffraction measurements at low temperatures. Stoichiometric $Tl_2Ru_2O_{7.00}$ synthesized under a high oxygen pressure of 3 GPa using $KClO_4$ shows a first-order metallic–semiconducting transition at 120 K. The high-temperature metallic phase has a cubic pyrochlore structure with a three dimensional network of both ruthenium and thallium. The low-temperature semiconducting phase has thallium sites with slightly short and long Tl–O distances, and the two Tl sites are ordered one dimensionally in the orthorhombic cell. Charge disproportionation of the Tl ions was suggested by valence bond sum calculations. By contrast, non-stoichiometric $Tl_2Ru_2O_{6.95}$ showed a spin-glass-like or canted-spin behavior around 40 K with resistivity increase also observed at this temperature. No significant structure changes were observed at the transition. Metallic–semiconducting transitions are discussed on the basis of their bond distance and angle changes.

1 Introduction

The pyrochlores $A_2Ru_2O_7$ exhibit a wide range of electrical resistivities: $Bi_2Ru_2O_7$ and $Pb_2Ru_2O_{6.5}$ are metallic and Pauli paramagnetic with low resistivities of $10^{-3}\ \Omega$ cm at room temperature; $Ln_2Ru_2O_7$ (Ln = Pr–Lu) and $Y_2Ru_2O_7$ are semiconducting with low activation energies;[1–3] and $Tl_2Ru_2O_{7-\delta}$ shows a metallic–semiconducting transition around 120 K.[4,5] To understand their high electrical conductivities, the electronic structures of $Bi_2Ru_2O_7$, $Y_2Ru_2O_7$, and $Pb_2Ru_2O_{6.5}$ have been investigated by XPS, UPS, and HREELS[6–8] and by the pseudofunction method.[9] The unoccupied Pb or Bi 6p states are close to E_F and contribute to the metallic conductivity by mixing with the Ru 4d state *via* the framework oxygen.

1.1 Thallium pyrochlores: synthesis, composition and properties

The thallium pyrochlore, $Tl_2Ru_2O_7$, was first synthesized by Sleight and Bouchard[4] using an applied pressure of 0.3 GPa and showed metallic properties with nearly temperature independent resistivity. Later, Jarrett *et al.*[5] reported that $Tl_2Ru_2O_{7-\delta}$ synthesized at high pressure showed a metallic–semiconducting transition around 120 K.

Previously, we have synthesized the thallium pyrochlore at atmospheric pressure and found a low-temperature phase, $Tl_2Ru_2O_7$ (synthesized at 773 K) and a high-temperature phase, $Tl_2Ru_2O_{6.71}$ (synthesized at 1173 K), which are semiconducting and metallic, respectively.[10] However, no metallic–semiconducting transition was observed around 120 K.

Systematic synthesis using high pressure and high oxygen pressure was recently performed.[11] The oxygen non-stoichiometry in the thallium pyrochlores is dependent on the synthesis conditions, with the ambiguity in physical properties reported previously[5] being caused by difficulties in the control of oxygen non-stoichiometry when reactions at atmospheric pressure are used. The results obtained by neutron diffraction experiments for the oxygen content are summarized as follows.[10,11] (i) The high temperature phase synthesized under atmospheric pressure shows a large number of oxygen vacancies with a stoichiometry of $Tl_2Ru_2O_{6.71}$ being obtained. (ii) The stoichiometric composition $Tl_2Ru_2O_7$ was obtained by applying high oxygen pressure using $KClO_4$ at 3 GPa. (iii) The high-pressure phase has a small amount of vacancy of 0.04(3) ($Tl_2Ru_2O_{6.96}$). (iv) The low-temperature phase synthesized under atmospheric pressure is stoichiometric, $\delta = 0$ ($Tl_2Ru_2O_7$).

Fig. 1 shows a typical behavior of electrical resistivities of these phases. The previous results are summarized as follows: (i) the high-temperature phase, $Tl_2Ru_2O_{6.71}$, is metallic. (ii) The high oxygen pressure phase, $Tl_2Ru_2O_7$, shows a metallic–semiconducting transition at 120 K. (iii) A small amount of oxygen vacancy in the structures, for example, in $Tl_2Ru_2O_{6.96}$ synthesized under high pressure shows a resistivity increase at the transition temperature around 40 K and (iv) the stoichiometric $Tl_2Ru_2O_7$ synthesized under atmospheric pressure is semiconducting.

Fig. 2 shows the temperature dependence of the magnetization for the thallium pyrochlores with various compositions. The stoichiometric $Tl_2Ru_2O_7$ synthesized under high oxygen pressure shows an abrupt change in magnetization at the transition temperature, which corresponds to the metallic–semiconducting transition. A small magnetization anomaly was also observed around 40 K. This anomaly might be caused either by another magnetic interaction or by an impurity phase with a lower oxygen content. The sample $Tl_2Ru_2O_{6.96}$, synthesized under high pressure showed the metallic-to-semiconducting change around 30–50 K, with a large difference between the field cooled and zero field cooled magnetization below the transition temperature, which is characteristic for a spin-glass-like behavior or canted antiferromagnet. The stoichiometric $Tl_2Ru_2O_7$ sample synthesized under atmospheric pressure shows a magnetization change near 120 K which corresponds

†Basis of the presentation given at Materials Chemistry Discussion No. 1, 24–26 September 1998, ICMCB, University of Bordeaux, France.

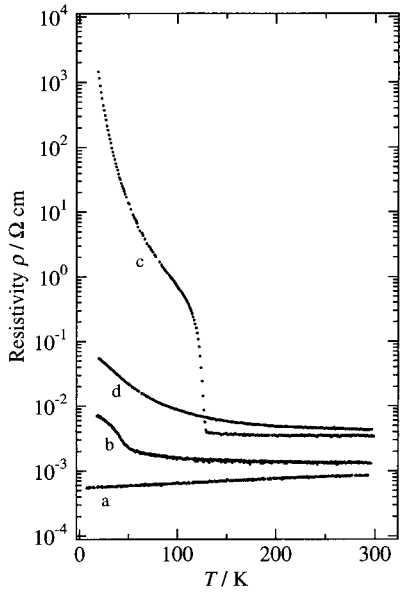

Fig. 1 Temperature dependence of the resistivity for the thallium pyrochlores. (a) $Tl_2Ru_2O_{6.71}$: high-temperature phase(HT), metallic; (b) $Tl_2Ru_2O_{6.96}$: high pressure phase, resistivity change around 50 K; (c) $Tl_2Ru_2O_7$: high oxygen pressure phase, metallic–semiconducting transition at 120 K; (d) $Tl_2Ru_2O_7$: low-temperature phase(LT), semiconducting.

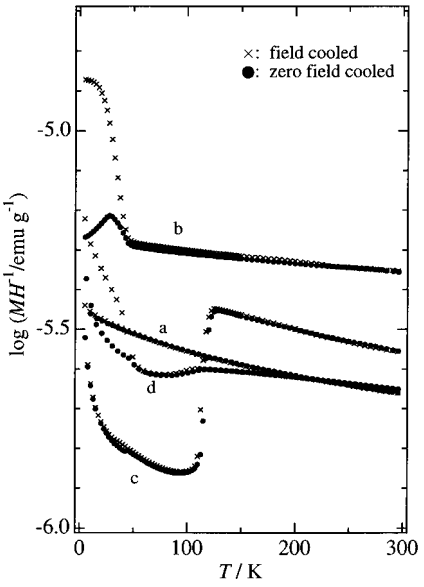

Fig. 2 Temperature dependence of the magnetization M/H for the thallium pyrochlores. (a) $Tl_2Ru_2O_{6.71}$: high-temperature phase(HT), metallic; (b) $Tl_2Ru_2O_{6.96}$: high pressure phase, resistivity change around 50 K; (c) $Tl_2Ru_2O_7$: high oxygen pressure phase, metallic–semiconducting transition at 120 K; (d) $Tl_2Ru_2O_7$: low-temperature phase (LT), semiconducting.

to the metallic–semiconducting transition of the high oxygen pressure phase, $Tl_2Ru_2O_7$. The difference between fc and zfc magnetization at $T<40$ K corresponds to the spin-glass-like behavior for $Tl_2Ru_2O_{6.96}$, and was also observed for $Tl_2Ru_2O_7$. The non-stoichiometric $Tl_2Ru_2O_{6.71}$ shows temperature independent magnetization in the temperature range observed.

1.2 Structure–property relationship

The relationships between the electrical properties and the crystal structures are also important factors to consider when discussing the property changes. Similarly to the cubic perovskite structure, the pyrochlores $A_2B_2O_6O'$ have a BO_3 array of

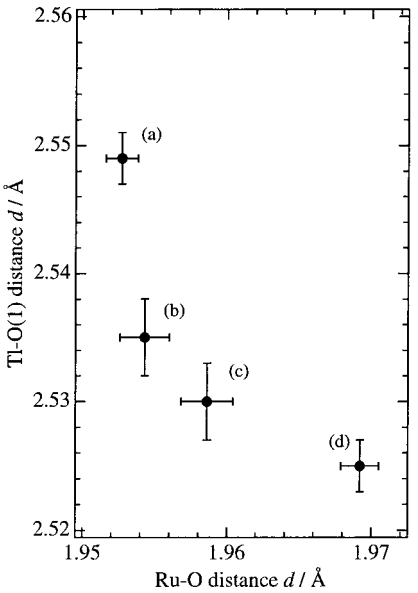

Fig. 3 Relations between the Ru–O distances and Tl-O(1) distances. (a) $Tl_2Ru_2O_{6.71}$: high-temperature phase, metallic; (b) $Tl_2Ru_2O_{6.96}$: high pressure phase, resistivity change around 50 K; (c) $Tl_2Ru_2O_7$: high oxygen pressure phase, metallic–semiconducting transition at 120 K; (d) $Tl_2Ru_2O_7$: low-temperature phase, semiconducting.

corner-shared octahedra, but the B–O–B angles are reduced from 180 to about 130°. Reduction of the B–O–B angles from 180° reduces the B–O–B overlap integrals, the electrical properties of the pyrochlores might thus be affected by a small change in the B–O–B angles.[12–18] Fig. 3 shows the relationship between the bond distances of the four samples indicated above as (i), (ii), (iii) and (iv). With increasing Ru–O(1) distances, the Tl–O(1) distance decreases, the Ru–O(1)–Ru angle decreases, and two O(1)–Ru–O(1) angles deviate from 90°. The increase in the Ru–O(1) bond lengths leads to the distortion of RuO_6 octahedra, and the reduction of Ru–O(1)–Ru angles, which tends to localize electrons owing to the reduced Ru–O(1) interaction.

The pyrochlore structure is viewed as being made up of two networks, $(Tl_2O)_\infty$ and $(RuO_3)_\infty$ which are interwoven with each other. The bridging oxide ions, O(1), are connected to both Tl and Ru ions, and the Tl–O(1) bond strength might strongly affect the Ru–O(1) bond. These two interactions are competitive; the stronger the Tl–O(1) bond, the weaker the Ru–O(1) bond.

1.3 Phase transition at low temperatures

X-Ray diffraction measurements at low temperatures, for the samples showing metallic–semiconducting transition at 120 K ($Tl_2Ru_2O_{7.0}$), show a discontinuity in the lattice parameters at the transition temperature. The transition was first-order, which is consistent with the hysteresis observed in the electrical and magnetic properties at the transition temperature. On the other hand, the slightly non-stoichiometric $Tl_2Ru_2O_{6.96}$ showed no significant anomaly in the lattice parameter curve at the transition, which is a possible indication of a higher order transition. However, the structure changes of the pyrochlores at the transition temperature are not clear.

In the current study, the thallium pyrochlores were synthesized under high pressure and high oxygen pressure conditions (1–5 GPa). The structures at low temperature were determined using neutron diffraction measurements, and the phase transitions in $Tl_2Ru_2O_7$ and $Tl_2Ru_2O_{6.96}$ were discussed together with the structural changes of other pyrochlores, $Ln_2Ru_2O_7$.

2 Experimental

The starting materials used in this study were RuO_2, Tl_2O_3, and Ru (RuO_2, Ru: Furuuchi Chemical Ind. Ltd., >99.99% purity; Tl_2O_3: Nakarai Chemicals Ltd. 99.9>% purity). The starting materials were weighed, mixed, and placed into a sandwich type gold capsule. The cell was then inserted in a piston-cylinder type high pressure apparatus and heated for 1 h at a fixed temperature of 1173 K and an applied pressure of 3 GPa. When high oxygen partial pressures were applied, the sample was placed into a gold capsule with $KClO_4$, either mixed with each other or separated with a stabilized ZrO_2 powder which prevented reaction between the oxides on both sides.

X-Ray diffraction patterns of the polycrystalline samples were obtained using a Rigaku RAD-C, 12 kW diffractometer with Cu-Kα radiation. The diffraction data were collected for 5 s at each 0.02° step width over a 2θ range from 10 to 100°. Neutron powder diffraction data were collected at 150, 100 and 2 K for $Tl_2Ru_2O_7$ synthesized at high-oxygen pressure, and 100 and 2 K for $Tl_2Ru_2O_{6.96}$ synthesized at high-pressure on the powder diffractometer D2B at ILL. The white beam of neutrons from the reactor was monochromatized to a wavelength of 1.5949 Å with a composite focusing Ge monochromator. Specimens of *ca.* 1 g were used for the measurements. The structural parameters were refined using RIETAN-97β.[19]

3 Results and discussion

3.1 Structures

3.1.1 $Tl_2Ru_2O_{7-\delta}$. A slightly oxygen deficient pyrochlore was synthesized at 1173 K and 3 GPa. The pyrochlore showed a gradual resistivity change around 50 K with a spin-glass-like behavior observed in the magnetization measurements. The composition of this sample was previously determined by the TOF neutron diffraction measurements and was deduced to be $Tl_2Ru_2O_{6.96}$.[10] The structure parameters were refined using neutron powder diffraction data at 100 and 2 K in this study. The diffraction patterns at 100 and 2 K were both indexed by a cubic cell with space group $Fd\bar{3}m$ (setting 2), and no extra reflections were observed in the patterns. Structural parameters were refined using the structural model, Tl at 16*d* (1/2, 1/2, 1/2), Ru at 16*c* (0, 0, 0) and O(1) at 48*f* (*x*, 1/8, 1/8) with $x \approx 0.32$, and O(2) at 8*b* (3/8, 3/8, 3/8). The site occupation parameters, *g*, of the Tl, Ru and O(2) sites were also refined; no significant deviation from the stoichiometric composition ($g=1$) was observed for the Tl, Ru and O(1) sites. In the final refinement cycle, anisotropic thermal parameters were assigned for all the sites. No correction was made for preferred orientation. Examination of the diffraction pattern at 2 K showed no evidence of superlattice reflections which indicated no symmetry changes at the transition temperature, no magnetic ordering was observed either. The structure at 100 K was then refined with the same model as that used previously.[11] Table 1 lists final *R* factors, lattice and structural parameters with their estimated standard deviations in parentheses. Table 2 gives interatomic distances and bond angles calculated with ORFFE.[20] Fig. 4 illustrates the profile fit and difference patterns for both samples. The occupancy at the O(2) site was determined to be 0.951(6) which gives the composition of the pyrochlore as $Tl_2Ru_2O_{6.951(6)}$. This is consistent with our previous results [$g=$ 0.96(3)] obtained from TOF neutron diffraction data at room temperature.

Fig. 5 shows the temperature dependence of the lattice

Table 1 Rietveld refinement results for $Tl_2Ru_2O_{6.95}$

(a) 100 K

Atom	Site	*g*	*x*	*y*	*z*	B/Å^2	U_{11}[c]/Å^2	U_{22}/Å^2	U_{33}/Å^2	U_{12}/Å^2	U_{13}/Å^2	U_{23}/Å^2
Tl	16*d*	1	1/2	1/2	1/2	0.36[b]	0.0045(12)	$=U_{11}$	$=U_{12}$	0.0003(11)	$=U_{12}$	$=U_{12}$
Ru	16*c*	1	0	0	0	0.36[b]	0.0045(12)	$=U_{11}$	$=U_{12}$	−0.0005(15)	$=U_{12}$	$=U_{12}$
O(1)	48*f*	1	0.3263(4)[a]	1/8	1/8	0.51[b]	0.011(2)	0.0044(12)	$=U_{22}$	0	0	−0.0017(16)
O(2)	8*b*	0.951(6)	3/8	3/8	3/8	0.43						

Space group $Fd\bar{3}m$, $a=10.171\,79(3)$ Å, $R_{wp}=3.75$, $R_p=2.80$, $S=R_{wp}/R_e=1.54$, $R_I=2.61$ and $R_F=1.92$.

(b) 2 K

Atom	Site	*g*	*x*	*y*	*z*	B/Å^2	U_{11}[c]/Å^2	U_{22}/Å^2	U_{33}/Å^2	U_{12}/Å^2	U_{13}/Å^2	U_{23}/Å^2
Tl	16*d*	1	1/2	1/2	1/2	0.20[b]	0.0025(11)	$=U_{11}$	$=U_{12}$	0.0010(11)	$=U_{12}$	$=U_{12}$
Ru	16*c*	1	0	0	0	0.31[b]	0.0040(9)	$=U_{11}$	$=U_{12}$	−0.0007(14)	$=U_{12}$	$=U_{12}$
O(1)	48*f*	1	0.3268(4)[a]	1/8	1/8	0.47[b]	0.011(2)	0.0034(11)	$=U_{22}$	0	0	0.0011(15)
O(2)	8*b*	0.951	3/8	3/8	3/8	0.43						

Space group $Fd\bar{3}m$, $a=10.16730(3)$ Å, $R_{wp}=3.62$, $R_p=2.78$, $S=R_{wp}/R_e=1.55$, $R_I=2.58$ and $R_F=2.21$.

[a]Numbers in parentheses are estimated standard deviations of the last significant digit. [b]Equivalent isotropic thermal parameter, B_{eq}. [c]The form of the anisotropic temperature factor is $\exp[-2\pi^2(h^2a^{*2}U_{11}+k^2b^{*}U_{22}+l^2c^{*}U_{33}+2hka^{*}b^{*}U_{11}+2hla^{*}c^{*}U_{13}+2klb^{*}c^{*}U_{23})]$.

Table 2 Interatomic distances (Å) and bond angles (°) for $Tl_2Ru_2O_{6.95}$. Symmetry relations: i x, $y+1/2$, $z+1/2$; ii $x-1/4$, $y+1/4$, $-z$; iii $-x+1/4$, $-y+1/4$, z; iv $-x+1/4$, y, $-z+1/4$; v x, $-y+3/4$, $-z+3/4$; vi x, $y-1/2$, $z-1/2$; vii $-x+3/4$, y, $-z+3/4$; viii $-z$, $x-1/4$, $y-1/4$

		Temperature/K		
		300	100	2
Tl–O(1)[i]	(×6)	2.535(3)	2.5215(7)	2.5172(7)
Tl–O(2)	(×2)	2.2047(1)	2.2026(1)	2.2017(1)
Ru–O(1)[ii]	(×6)	1.9543(17)	1.9584(4)	1.9598(4)
Ru[iii]–O(1)–Ru[iv]		134.2(2)	133.32(5)	133.07(5)
Tl[v]–O(1)–Tl[vi]		90.48(14)	90.99(3)	91.14(3)
Tl[v]–O(1)–Tl[vii]		109.4712	109.4712	109.4712
O(1)[ii]–Ru–O(1)[viii]		94.75(15)	95.33(3)	95.94(3)

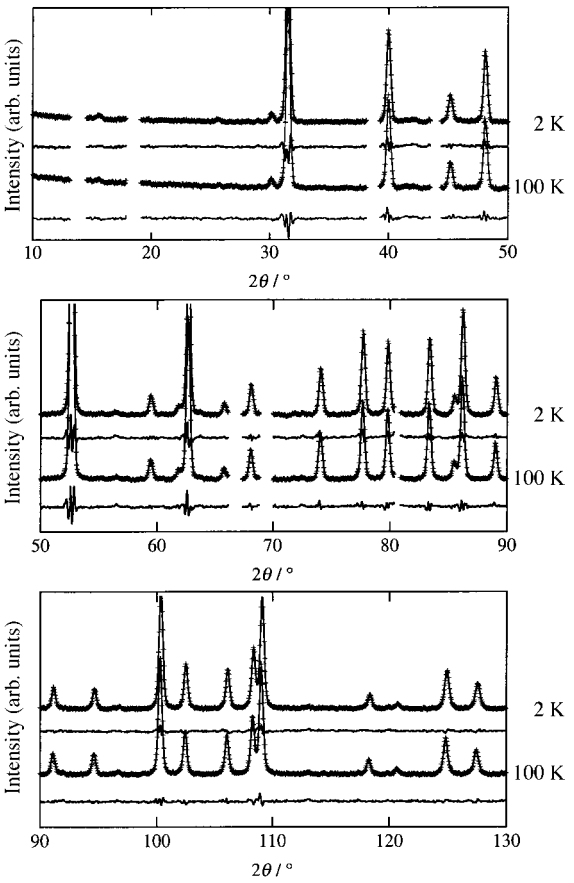

Fig. 4 Observed, calculated, and difference plots for the neutron Rietveld analysis for $Tl_2Ru_2O_{6.95}$ at 100 K (a) and 2 K (b). The solid line depicts calculated intensities, and the overlying + the observed intensities. The difference between the observed and calculated intensities is also indicated. The excluded regions contained peaks due to the instrumentation.

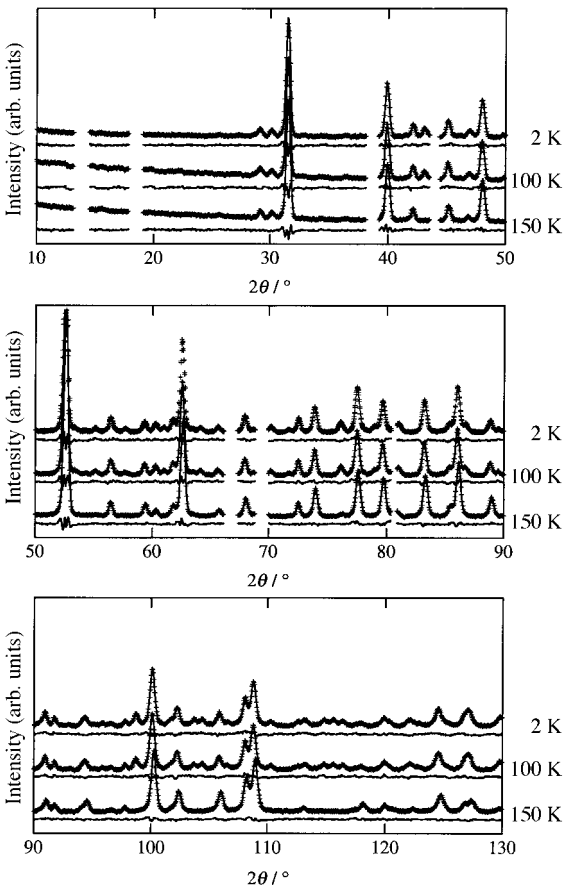

Fig. 6 Observed, calculated, and difference plots for the neutron Rietveld analysis for $Tl_2Ru_2O_7$ at 150 K (a), 100 K (b), and 2 K (c). The solid line depicts calculated intensities, and the overlying + the observed intensities. The difference between the observed and calculated intensities is also indicated. The excluded regions contained peaks due to the instrumentation.

parameters for $Tl_2Ru_2O_{6.95}$. The results were obtained from both X-ray and neutron diffraction data. The parameters determined using the neutron and X-ray diffraction data are consistent with each other.

With decreasing temperature, the Tl–O(1) and Tl–O(2) distances decrease from 2.535(3) and 2.2047(1) Å (300 K) to 2.5172(7) and 2.2017(1) Å (2 K), respectively, while the Ru–O distance increases slightly from 1.9543(17) Å (300 K) to 1.9598(4) Å (2K). The Ru–O–Ru angle decreases from 134.2(2)° (300K) to 133.07(5)° (2 K). These structural

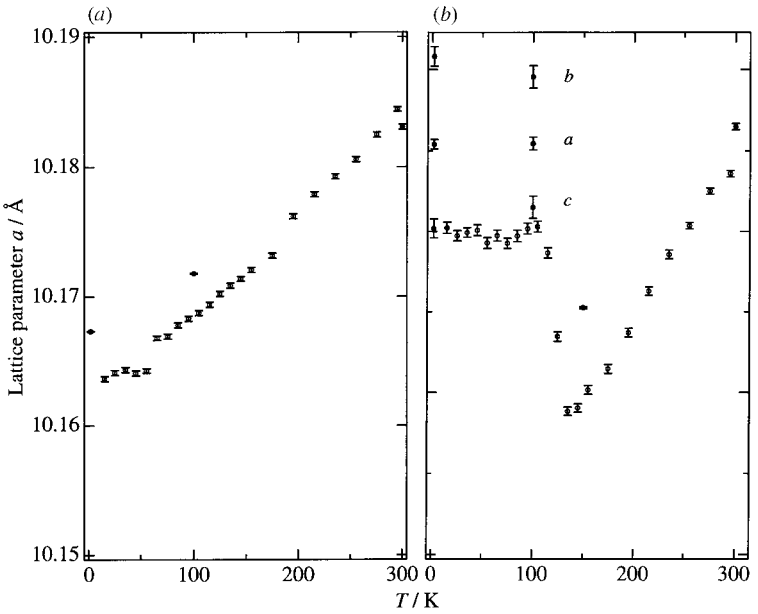

Fig. 5 Temperature dependence of the lattice parameters for $Tl_2Ru_2O_{6.95}$ (a) and $Tl_2Ru_2O_7$ (b) determined by the X-ray (○) and neutron (●) diffraction measurements.

changes are consistent with the property change from metallic to semiconducting with decreasing temperature, and are similar to those observed for other $A_2Ru_2O_7$ pyrochlores.[12–18]

Reimers *et al.*[21] found short range magnetic ordering for the pyrochlores $Tb_2Mo_2O_7$ and $Y_2Mn_2O_7$ using the difference plots of the neutron diffraction data between the high temperature non-magnetic state and the low-temperature magnetic ordering state. Similar plots were examined using the diffraction data at 100 and 2 K. However, no significant peaks were observed in the difference plots.

3.1.2 $Tl_2Ru_2O_7$. The stoichiometric pyrochlore, $Tl_2Ru_2O_7$, was synthesized at 1173 K and 3 GPa with $KClO_4$. The sample showed a metallic–semiconducting transition at 120 K. The structural parameters were determined using neutron powder diffraction data at 150, 100 and 2 K. The diffraction pattern at 150 K indexed as a cubic cell and the parameters were refined in space group $Fd\bar{3}m$ (setting 2) using the same structural model as $Tl_2Ru_2O_{6.951}$. The site occupation parameters, g, of the Tl, Ru and O(2) sites were also refined; no significant deviation from the stoichiometric composition was observed for the Tl [$g=1.000(2)$] and O(1) [$g=1.000(6)$] sites. In the final refinement cycle, anisotropic thermal parameters were assigned for all the sites. No correction was made for preferred orientation.

The diffraction pattern at 100 K also indicated a cubic cell with $a=10.17$ Å, similar to that of 150 K. However, small reflections were observed and are indexed by the same cell as the parent cubic cell. No extinction rules were observed in this cubic cell. Previously, we observed the superlattice reflections by low-temperature X-ray diffraction measurements, and the reflections were consistent with those observed in the neutron diffraction measurements.[11] This indicates a first order crystallographic phase transition. The refinements were carried out using several structural models with lower symmetry, such as $P4\bar{3}m$, and $P4m2$. However, these models did not lead to low R values.

Several structural models have been proposed based on the ordering in the metal ions in the pyrochlore structure. For example, one dimensional ordering of the metal ions sites was reported for the fluoride pyrochlores, $NH_4Fe_2F_4$, where the Fe^{3+} and Fe^{2+} ions are ordered one dimensionally along the $\langle 010\rangle$ and $\langle 100\rangle$ directions, respectively, in the orthorhombic cell with space group *Pnma*.[22] This model was then considered for the low-temperature structure. In the space group *Pnma*, both Tl and Ru sites divided into two, and these two sites ordered one dimensionally. The 48*f* O site is divided into four sites. The relation between the cubic and the new orthorhombic cell is as follows: $a_o \approx b_o \approx a_c/2^{1/2}$, and and $c_o \approx c_c$. Refinements using this structural model led to a significant reduction in the R values, and all superlattice reflections were explained by this model. The diffraction pattern at 2 K also shows the same superlattice reflections as that of 100 K, and no magnetic reflections were observed. The refinements were carried out with the same structural model. Fig. 6 shows the profile fit and difference patterns of $Tl_2Ru_2O_7$ at 150, 100, and 2 K. The refinement results at 150, 100, and 2 K are given in Table 3 and bond distances and angles are listed in Table 4.

The temperature dependence of the lattice parameters for the thallium pyrochlores is shown in Fig. 5. For the stoichio-

Table 3 Rietveld refinement results for $Tl_2Ru_2O_7$

(a) 150 K
$Tl_2Ru_2O_7$

Atom	Site	g	x	y	z	B/Å^2	U_{11}[c]/Å^2	U_{22}/Å^2	U_{33}/Å^2	U_{12}/Å^2	U_{13}/Å^2	U_{23}/Å^2
Tl	16*d*	1	1/2	1/2	1/2	0.48[b]	0.0061(3)	$=U_{11}$	$=U_{12}$	0.0002(3)	$=U_{12}$	$=U_{12}$
Ru	16*c*	1	0	0	0	0.24[b]	0.0030(3)	$=U_{11}$	$=U_{12}$	−0.0006(4)	$=U_{12}$	$=U_{12}$
O(1)	48*f*	1	0.32684(10)[a]	1/8	1/8	0.48[b]	0.0095(5)	0.0043(3)	$=U_{22}$	0	0	0.0011(4)
O(2)	8*b*	1	3/8	3/8	3/8	0.50						

Space group $Fd\bar{3}m$, $a=10.17528(5)$ Å, $R_{wp}=3.08$, $R_p=2.33$, $S=R_{wp}/R_e=1.37$, $R_I=2.04$ and $R_F=1.40$.

RuO_2[d]

Atom	Site	g	x	y	z	B/Å^2
Ru	2*a*	1	0	0	0	0.32(17)
O	4*f*	1	0.3054(6)	$=x$	0	0.21(17)

$a=4.48814(17)$ Å, $c=3.10589(16)$ Å, $R_I=5.85$ and $R_F=3.91$.

(b) 100 K

Atom	Site	g	x	y	z	B/Å^2
Tl(1)	4*a*	1	0	0	1/2	0.60(7)
Tl(2)	4*c*	1	0.2497(7)	1/4	0.7709(5)	0.24(10)
Ru(1)	4*a*	1	0	0	0	0.21(8)
Ru(2)	4*c*	1	0.2315(13)	1/4	0.2550(5)	0.51(11)
O(1)	4*c*	1	−0.0180(11)	1/4	0.3524(9)	0.27(3)
O(2)	4*c*	1	0.0064(12)	1/4	0.9274(9)	$=$O(1)
O(3)	8*d*	1	0.1761(6)	0.4395(8)	0.1342(7)	$=$O(1)
O(4)	8*d*	1	0.7792(8)	0.4538(8)	0.1222(6)	$=$O(1)
O(5)	4*c*	1	0.5173(10)	1/4	0.8745(12)	$=$O(1)

space group *Pnma*, $a=7.2022(4)$ Å, $b=7.2051(5)$ Å, $c=10.1815(7)$ Å, $R_{wp}=3.47$, $R_p=2.68$, $S=R_{wp}/R_e=1.58$, $R_I=2.50$ and $R_F=1.70$.

(c) 2 K

Site	g	x	y	z	B/Å^2
4*a*	1	0	0	1/2	0.61(6)
4*c*	1	0.2483(5)	1/4	0.7719(5)	0.10(8)
4*a*	1	0	0	0	0.06(6)
4*c*	1	0.2296(11)	1/4	0.2539(4)	0.33(9)
4*c*	1	−0.0201(10)	1/4	0.3547(8)	0.15(3)
4*c*	1	0.0063(10)	1/4	0.9301(7)	$=$O(1)
8*d*	1	0.1748(6)	0.4416(7)	0.1342(6)	$=$O(1)
8*d*	1	0.7798(7)	0.4561(7)	0.1218(6)	$=$O(1)
4*c*	1	0.5172(9)	1/4	0.8759(10)	$=$O(1)

Space group *Pnma*, $a=7.2022(3)$ Å, $b=7.2060(5)$ Å, $c=10.1802(6)$ Å, $R_{wp}=3.70$, $R_p=2.91$, $S=R_{wp}/R_e=1.54$, $R_I=2.35$ and $R_F=1.47$.

[a]Number in parentheses are estimated standard deviations of the last significant digit. [b]Equivalent isotropic thermal parameter, B_{eq}. [c]The form of the anisotropic temperature factor is $\exp[-2\pi^2(h^2a^{*2}U_{11}+k^2b^{*2}U_{22}+l^2c^{*2}U_{33}+2hka^*b^*U_{11}+2hla^*c^*U_{13}+2klb^*c^*U_{23})]$. [d]Refinement using space group $P4_2/mnm$.

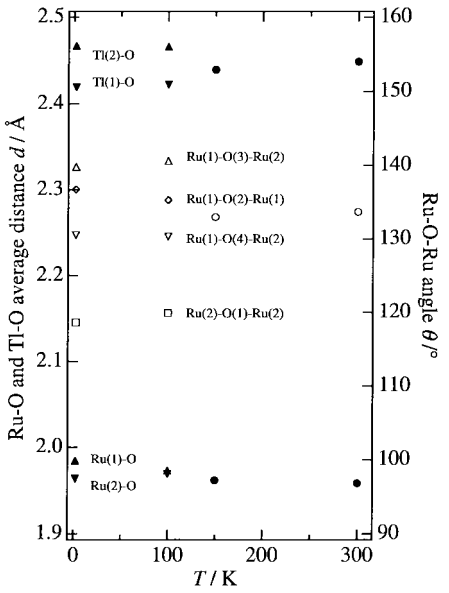

Fig. 7 Temperature dependence of the average Tl–O and Ru–O distances in $Tl_2Ru_2O_7$.

metric $Tl_2Ru_2O_7$, a large increase in the lattice parameters was observed at the transition temperature, 120 K. This is explained by a first order crystallographic phase transition which is consistent with the hysteresis observed in the electrical and magnetic data near the transition temperature.

Fig. 7 shows the temperature dependence of the atomic distances and angles. The average values of Tl(1)–O, Tl(2)–O, Ru(1)–O and Ru(2)–O distances are indicated for the low-temperature phase. The Ru–O distances increase slightly from 1.9619(4) to 1.969 Å from 150 to 100 K, and the increase in the Ru–O distance corresponds to the metallic to semiconducting transition. On the other hand, the Tl–O distances decrease slightly from 2.449 to 2.439 Å from 300 to 150 K, and then split into two, shorter (2.422 Å) and longer (2.466 Å) distances below the metallic-semiconducting transition temperature. Larger splitting for the Tl sites may indicate charge disproportionation of the Tl ions.

To address the electronic implications of these structural changes, valence bond sums and Madelung site potentials have been calculated using the program EUTAX.[23] Fig. 8 illustrates

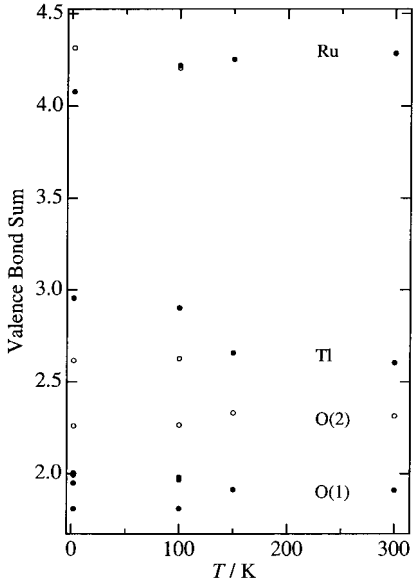

Fig. 8 Valence bond sums of $Tl_2Ru_2O_7$ as a function of the temperature.

Table 4 Interatomic distances (Å) and bond angles (°) for $Tl_2Ru_2O_7$[a] 300 and 150 K

		Temperature/K	
		300	150
Tl–O(1)[i]	(×6)	2.530(3)	2.5181(8)
Tl–O(2)	(×2)	2.2054(1)	2.2035(1)
Ru–O(1)[ii]	(×6)	1.9586(18)	1.9619(4)
Ru[iii]–O(1)–Ru[iv]		133.7(2)	132.99(5)
Tl[v]–O(1)–Tl[vi]		90.78(15)	91.19(3)
Tl[v]–O(1)–Tl[vii]		109.4712	109.4712
O(1)[ii]–Ru–O(1)[viii]		95.09(17)	95.55(3)

100 and 2 K

		Temperature/K	
		100	2
Ru(1)–O(2)	(×2)	1.948(3)	1.938(3)
Ru(1)–O(3)	(×2)	1.914(7)	1.911(6)
Ru(1)–O(4)	(×2)	2.046(7)	2.042(6)
average Ru(1)–O		1.969	1.964
Ru(2)–O(1)		2.052(12)	2.069(11)
Ru(2)–O(1)		2.110(13)	2.121(11)
Ru(2)–O(3)	(×2)	1.880(7)	1.878(6)
Ru(2)–O(4)	(×2)	1.959(7)	1.978(7)
average Ru(2)–O		1.973	1.984
O(2)–Ru(1)–O(4)		84.3(3)	84.5(3)
O(2)–Ru(1)–O(3)		87.4(2)	87.5(2)
O(3)–Ru(1)–O(4)		87.5(3)	87.7(2)
O(1)–Ru(2)–O(3)		97.5(5)	98.1(4)
O(1)–Ru(2)–O(4)		81.1(2)	81.0(2)
O(1)–Ru(2)–O(3)		81.0(4)	80.7(3)
O(1)–Ru(2)–O(4)		100.4(4)	100.2(3)
O(3)–Ru(2)–O(4)		84.9(3)	84.3(2)
O(3)–Ru(2)–O(3)		93.1(4)	94.4(3)
O(4)–Ru(2)–O(4)		97.1(4)	97.0(4)
Ru(1)–O(2)–Ru(1)		135.3(4)	136.7(4)
Ru(2)–O(1)–Ru(2)		119.9(5)	118.6(4)
Ru(1)–O(3)–Ru(2)		140.6(4)	139.8(3)
Ru(1)–O(4)–Ru(2)		130.3(3)	130.5(3)

		Temperature/K	
		100	2
Tl(1)–O(1)	(×2)	2.349(6)	2.333(5)
Tl(1)–O(3)	(×2)	2.739(5)	2.746(4)
Tl(1)–O(4)	(×2)	2.388(6)	2.390(5)
Tl(1)–O(5)	(×2)	2.212(7)	2.207(6)
average Tl(1)–O		2.422	2.419
Tl(2)–O(2)		2.368(10)	2.377(9)
Tl(2)–O(2)		2.738(9)	2.766(8)
Tl(2)–O(3)	(×2)	2.688(6)	2.682(5)
Tl(2)–O(4)	(×2)	2.405(3)	2.390(5)
Tl(2)–O(5)		2.197(12)	2.207(10)
Tl(2)–O(5)		2.235(10)	2.238(8)
average Tl(2)–O		2.466	2.467

the variation in the valence bond sums for Tl, Ru, O(1) and O(2) as a function of temperature. The results obtained at 300 K were calculated from the TOF neutron diffraction data.[11] Below the metallic–semiconducting transition temperature of 120 K, Tl and Ru sites divided into two sites. At 100 K, the valence values of the two Tl sites were 2.6 and 2.9, respectively, while the two Ru sites gave very similar valence values. The valence sum calculation also suggests charge disproportionation for Tl at the metallic–semiconducting transition with $2Tl^{m+} \leftrightarrow Tl^{m-\delta} + Tl^{m+\delta}$. Fig. 9 shows the structure of $Tl_2Ru_2O_7$ at 100 K. In this structure, Tl and Ru sites are divided into two sites with a 1:1 ratio. Two Tl sites

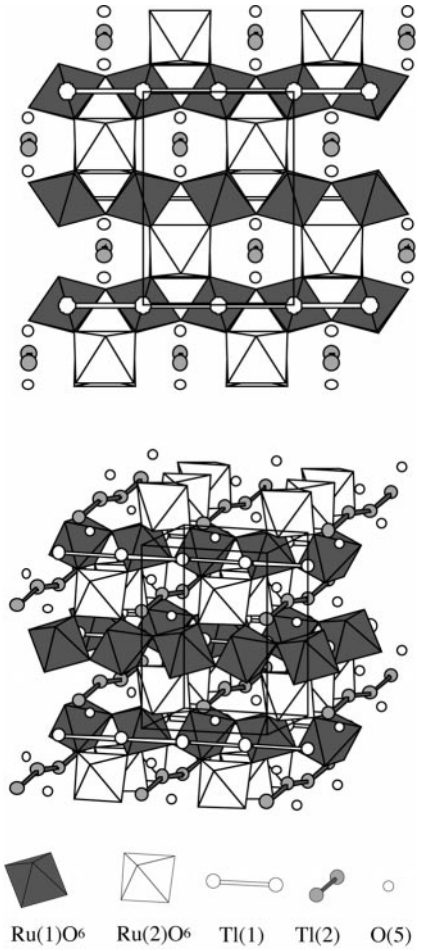

Fig. 9 Structure of $Tl_2Ru_2O_7$ at 100 K.

correspond to $Tl^{m-\delta}$ and $Tl^{m+\delta}$ which are ordered one dimensionally.

3.2 Structure–property relationships in pyrochlores

We previously proposed that metallic ruthenate pyrochlores are characterized by relatively short Ru–O bonds (*ca.* 1.95 Å) compared with *ca.* 1.98 Å in the semiconducting analogues, and more open Ru–O–Ru angles, 130–140° for metallic species *versus* 129–134° for semiconducting oxides. The effect of smaller Ru–O distances and larger Ru–O–Ru angles is to increase the overlap between the Ru 4d and O 2p orbitals. For example, in $Bi_{2-x}Ln_xRu_2O_7$ and $Pb_{2-x}Ln_xRu_2O_{7-\delta}$ (Ln = Pr–Lu, Y) solid solutions,[12–14] the resistivity increases with x, and the metallic property changes to semiconducting between $x = 1.2$ and 1.4. The Ru–O(1) bond lengths, the distortion of the RuO_6 octahedra, and the bend in the RuO_6 zigzag chains increase from $x = 0$ to 2.0. These structural changes are quite similar to those found in the thallium pyrochlores.

More precise structural data were obtained using neutron diffraction,[16–18] which enables a detailed study of the structural features in metallic *versus* semiconducting ruthenate pyrochlores. They concluded that while the difference in the Ru–O bond distances between the two systems is small, Ru–O–Ru angles greater than 133° are undoubtedly necessary to obtain metallic conductivity.

Thallium ruthenate pyrochlore is the only system which shows metallic, semiconducting and metallic–semiconducting transition, depending on the amount of oxygen vacancies.

Fig. 10 summarizes the Ru–O(1) bond distances, Ru–O(1)–Ru angles and valence bond sums as a function of lattice parameters for the Ru-containing pyrochlores. The data are taken from our previous X-ray Rietveld refinement results[12,13] and also from the results obtained from neutron diffraction experiments.[16,24,25] The bond distances obtained from the X-ray and neutron diffraction experiments are consistent with each other, except for the bismuth pyrochlore as indicated by Kennedy and Vogt.[16] This might be caused by the difference in the sample stoichiometry; the bismuth ruthenate used for the neutron structure analysis contained O(2) deficiency with the composition determined as $Bi_2Ru_2O_{6.92}$.[24]

The metallic region is obviously separated from the semiconducting region; compounds with Ru–O(1) distances of 1.94–1.97 Å and Ru–O(1)–Ru angles of 134–139° show metallic behavior, and those with Ru–O(1) distances of 1.97–2.00 Å and Ru–O(1)–Ru angles of 129–134° show semiconducting behavior. The bond distances and bond angles determined for $Tl_2Ru_2O_{7-\delta}$ correspond to the borderline between metallic and semiconducting behavior.

The valence bond sum of these pyrochlores is also indicated in Fig. 10. Deviation from the linear relationship with the lattice parameters was observed for Tl and Bi pyrochlores. This might indicate the importance of the interaction between the Bi or Tl, and the oxygen, which leads to metallic properties for the pyrochlores. Further study on the electronic structure of the thallium pyrochlores is necessary.

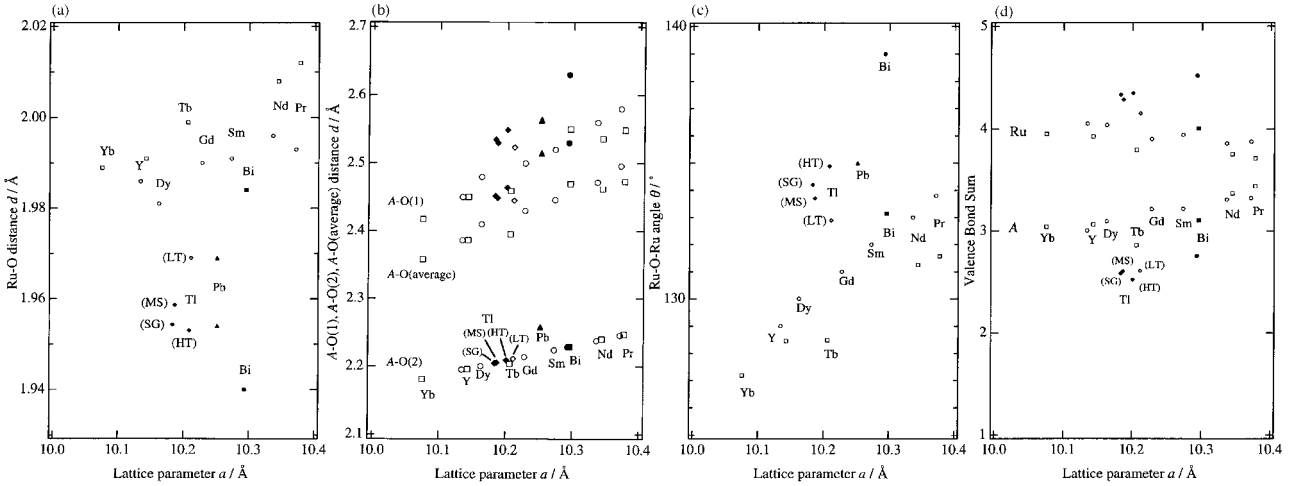

Fig. 10 The Ru–O bond distances (a), the Tl–O bond distances (b), the Ru–O–Ru angles (c) and valence bond sums (d) as a function of lattice parameters for $A_2Ru_2O_{7-\delta}$. (●) samples showing metallic property; (○) samples showing semiconducting property; (◇) samples showing metallic–semiconducting transition; Tl(HT): $Tl_2Ru_2O_{6.71}$; Tl(LT): $Tl_2Ru_2O_7$, low-temperature phase; Tl(SG): $Tl_2Ru_2O_7$, high pressure phase; Tl(MS): $Tl_2Ru_2O_7$, high oxygen pressure phase.

References

1 R. J. Bouchard and J. L. Gillson, *Mater. Res. Bull.*, 1971, **6**, 69.
2 J. M. Longo, P. M. Raccah and J. B. Goodenough, *Mater. Res. Bull.*, 1969, **4**, 191.
3 R. Aleonard, A. F. Berthand, M. C. Montomry and R. Pauthenet, *J. Appl. Phys.*, 1962, **33**, 1205.
4 A. W. Sleight and R. J. Bouchard, *Solid State Chemistry, Proceedings of 5th Materials Research Symposium, July 1972*, NBS Spec. Publ. 364, p. 227.
5 H. S. Jarrett, A. W. Sleight, J. F. Weiher, J. L. Gillson, C. G. Frederick, G. A. Jones, R. S. Swingle, D. Swartzfager, J. E. Gulley and P. C. Hoell, *Valence Instabilities and Related Narrow-Band Phenomena*, ed. R. D. Parks, Plenum, New York, 1977, p. 545.
6 J. B. Goodenough, A. Hamnett and D. Telles, *Localization and Metal–Insulator Transition*, ed. H. Fritzshe and D. Adler, Plenum, New York, 1985, p. 161.
7 P. A. Cox, J. B. Goodenough, P. J. Tavener, D. Telles and R. G. Egdell, *J. Solid State Chem.*, 1986, **62**, 360.
8 P. A. Cox, R. G. Egdell, J. B. Goodenough, A. Hamnett and C. C. Naish, *J. Phys. C*, 1983, **16**, 6221.
9 W. Y. Hsu, R. V. Kasowski, T. Miller and T.-C. Chiang, *Appl. Phys. Lett.*, 1988, **52**, 792.
10 R. Kanno, J. Huang and A. W. Sleight, *Proceedings of the Fifth International Symposium on Advanced Nuclear Energy Research, Neutrons as Microscopic Probes, March 1993*, JAERI-M 93, 228, vol. 2, p. 347.
11 T. Takeda, M. Nagata, H. Kobayashi, R. Kanno, Y. Kawamoto, M. Takano, T. Kamiyama, F. Izumi and A. W. Sleight, *J. Solid State Chem.*, in press.
12 R. Kanno, Y. Takeda, T. Yamamoto, Y. Kawamoto and O. Yamamoto, *J. Solid State Chem.*, 1993, **102**, 106.
13 T. Yamamoto, R. Kanno, Y. Takeda, O. Yamamoto, Y. Kawamoto and M. Takano, *J. Solid State Chem.*, 1994, **109**, 372.
14 H. Kobayashi, R. Kanno, Y. Kawamoto, T. Kamiyama, F. Izumi and A. W. Sleight, *J. Solid State Chem.*, 1995, **114**, 15.
15 K.-S. Lee, D.-K. Seo and M.-H. Whangbo, *J. Solid State Chem.*, 1997, **131**, 405.
16 B. J. Kennedy and T. Vogt, *J. Solid State Chem.*, 1996, **126**, 261.
17 B. J. Kennedy, *J. Solid State Chem.*, 1995, **119**, 254.
18 B. J. Kennedy, *J. Solid State Chem.*, 1996, **123**, 14.
19 F. Izumi, *The Rietveld Method*, ed. R. A. Young, Oxford Univ. Press, Oxford, 1993, ch. 13.
20 W. R. Busing, K. O. Martin and H. A. Levy, Report ORNL-TM-306, Oak Ridge National Laboratory, Oak Ridge, TN, 1964.
21 J. N. Reimers, J. E. Greedan and M. Sato, *J. Solid State Chem.*, 1988, **72**, 390.
22 G. Ferey, M. Leblanc and R. De Pape, *J. Solid State Chem.*, 1981, **40**, 1; G. Ferey, M. Leblanc, R. De Pape and J. Pannetier, *Solid State Commun.*, 1985, **53**, 559.
23 M. O'Keeffe, EUTAX, Version 1.3 EMlab Software, Phoenix, AZ, 1993.
24 G. R. Facer, M. M. Elcombe and B. J. Kennedy, *Aust. J. Chem.*, 1993, **46**, 1897.
25 R. A. Beyerlein, H. S. Horowitz, J. M. Longo, M. E. Leonowicz, J. D. Jorgensen and F. J. Rotella, *J. Solid State Chem.*, 1984, **51**, 253.

Paper 8/05664A